Engineering Analysis with Boundary Elements 41 (2014) 103–110

Contents lists available at ScienceDirect

Engineering Analysis with Boundary Elements

journal homepage: www.elsevier.com/locate/enganabound

Adsorption in honeycomb adsorber by BEM

T. Štimec [a], M. Hriberšek [b], J. Ravnik [b,*], S. Bašič [a]

[a] Esotech d.d., Preloška cesta 1, SI-3320 Velenje, Slovenia
[b] Faculty of Mechanical Engineering, University of Maribor, Smetanova 17, SI-2000 Maribor, Slovenia

ARTICLE INFO

Article history:
Received 18 October 2013
Accepted 9 January 2014

Keywords:
Subdomain boundary element method
Laminar viscous fluid flow
Mass transfer
Adsorption
Honeycomb adsorber

ABSTRACT

A computational scheme based on the subdomain Boundary Element Method is presented for the numerical simulation of the adsorption process in a honeycomb adsorber. Incompressible flow of air mixed with a very low concentration ($<1\%$) of n-butane in a carbon coated adsorber channel is considered. A new model accounting for the mass transfer due to the adsorption process at the channel walls is presented. A diffusion–convection transport equation for species transport is solved for the mass transfer in the fluid, whereas the mass transfer from the fluid phase to the solid phase, driven by the adsorbent concentration gradient near the wall, which takes place until adsorption equilibrium is reached in the adsorbent layer, is modelled in a form of a dynamic boundary condition for adsorbent concentration. Adsorption equilibrium is calculated with the use of the Dubinin–Radushkevich equilibrium model. Due to very low concentration, the isothermal case is computed and the break-through concentration curves at the outlet of the adsorber channel are compared with experimental and computational results. A detailed analysis of local values of the Sherwood number, concentrations at the wall and partitioning coefficient at different *Re* number values shows that the proposed numerical model accurately predicts the adsorption dynamics inside a honeycomb adsorber, and can be extended to other types of surface adsorbers.

1. Introduction

Adsorption process and adsorption based technologies have enjoyed much attention in the past and a wide range of different scientific studies were performed in this field. Because of the engineering importance most of the works was done in the field of adsorption equilibrium modelling [16,21,9,27] or in the field of adsorption processes and interactions of heat and mass transfer in packed bed adsorbers [4,5,20]. Adsorption equilibrium modelling is traditionally described by simple analytical models such as Henry, Langmuir or Freundlich isotherms, and was in the last decade advanced with the development of Monte Carlo (MC) simulations and Molecular Dynamics (MD) simulations, as noted in [8]. Accuracy of MD simulations is in most cases remarkable, but this technique still did not enter engineering applications on a wide scale. The main reason for that can be found in the amount of computer resources it demands, the complexities associated with this kind of modelling and with the lack of information about adsorbent/adsorbate properties. For engineering calculations empirical models, for example the Dubinin–Radushkevich model, are still the preferred choices over more complex MC and MD simulations [6,23]. Adsorption technologies also gained some new attention, especially with new types of special adsorbers that do not feature adsorbent material in a packed bed form. In case of a honeycomb adsorber the adsorbent material is attached to the honeycomb structure as a thin film on the surfaces of the channels [22], ensuring fast mass exchange rates between the bulk flow and the adsorbent walls. Because of the simple channel geometry the pressure drop is much lower, which together with a possibility of very short time intervals for cycling of adsorption/desorption processes drives the research in the field of honeycomb adsorbers [24,10,11,26,25].

The Boundary Element Method (BEM) and its variants possess an advantage over other members of approximation methods in the form of a direct computation of function and its normal derivatives on the boundary of the domain. Since in the present case the most important physical phenomenon – the adsorption of species – is occurring at the wall, direct computation of function derivatives could be used in order to simplify and improve computation of adsorption mass fluxes at the solid walls. In the BEM context, passive convection–diffusion mass transfer was accounted for in [19,14,1], mainly in the context of species concentration influenced buoyancy force. When using the subdomain version of BEM for the solution of velocity–vorticity formulation of Navier–Stokes equations, the main disadvantage of BEM is

* Corresponding author. Tel.: +386 2 220 7745; fax: +386 2 220 7996.
E-mail addresses: teodor@stimec.si (T. Štimec), matjaz.hribersek@um.si (M. Hriberšek), jure.ravnik@um.si (J. Ravnik), sani.basic@esotech.si (S. Bašič).

0955-7997/$ - see front matter © 2014 Elsevier Ltd. All rights reserved.
http://dx.doi.org/10.1016/j.enganabound.2014.01.010

accounted for, as sub-domain BEM leads to sparse system of equations. In the present case of adsorption phenomenon inside the honeycomb channels, which is influenced by both mass transfer mechanisms, the subdomain BEM for simple mass transfer problems in fluids is therefore extended to mass transfer problems with fluid-wall interaction in the form of adsorption. Since adsorption mass transfer stops, when equilibrium conditions are reached, special attention has to be paid to proper incorporation of equilibrium conditions on the solid walls, presenting the interface between the fluid and the solid phase. There is however an additional problem, associated with adsorption in the phase when equilibrium conditions are not yet established, namely a proper definition of the driving force in the form of concentration difference between the solid wall and the surrounding fluid. Here, a physically correct model for the varying concentration values on the solid wall plays the most important role. To solve this problem, a quasi-equilibrium model is introduced, which enables a dynamic adaptation of the concentration boundary values according to the already adsorbed adsorbent mass.

The paper is organized as follows. After a short description of the adsorbent geometry, mixture flow and physical properties, governing equations are explained, followed by definition of initial and boundary conditions. A special attention is given to boundary and equilibrium conditions at the wall. Next, the Boundary Element Method based transformation of the governing equations into the final nonlinear system of algebraic equations is described in detail. A summary of the numerical procedure and simulation details precedes Section 5, where the derived numerical algorithm is applied for a computational parametric study of the adsorption process in the honeycomb channel. The paper closes with conclusions.

2. Problem description

A honeycomb adsorption channel is schematically shown in Fig. 1. As the carrier gas with an adsorbate species enters the honeycomb channel, a fraction of adsorbate molecules is absorbed by the adsorbent materials on channel surfaces. Adsorbed molecules penetrate into the pore system of adsorbent material and form a thin film on active surfaces of adsorbent due to short range attractive forces between active surfaces of solid adsorbent and adsorbate molecules. Diffusion processes in adsorbent materials are still not well explained but equilibrium times for adsorption processes are known to be in a range of several μs. Therefore the diffusion processes of adsorbate molecules in the bulk fluid towards adsorbent material on the channel walls are the rate controlling mechanism. The model presented is based on the following conditions: (1) the flow is isothermal, incompressible and laminar, (2) species concentration is low, (3) buoyancy forces, thermal diffusion, diffusion-thermo (Dufour), interdiffusion effects are neglected, (4) viscous heat dissipation, thermal radiation, pressure work are also neglected in comparison to advection. Since the amount of adsorbed species is negligibly small in comparison to the mass flow rate of carrier gas it is assumed that the adsorption process does not affect the flow field in the channel. For a solid adsorbent it is assumed that it has a micropore system and it is non-porous for the carrier fluid flow. As such, it is not geometrically included in flow calculations.

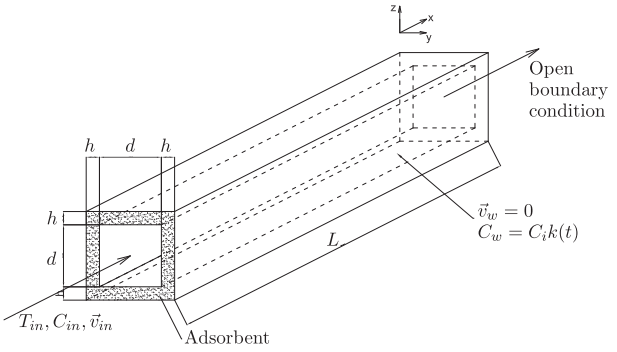

Fig. 1. Sketch of a single honeycomb channel. The length of the channel is $L=50$ mm, the width of the channel is $d=1.5$ mm and the thickness of the adsorbent layer is $h=0.015$ mm.

3. Governing equations

3.1. Fluid flow and mass transfer

The air mixture is considered as an incompressible fluid with constant physical properties' density $\rho_0 = 1.164\ \mathrm{kg/m^3}$ and kinematic viscosity $\nu_0 = 1.522 \times 10^{-5}\ \mathrm{m^2/s}$. Due to the adsorption phenomena, the species in the form of butane is transported within the mixture by means of convection and diffusion, and is adsorbed or desorbed on the walls. Species diffusivity $D_0 = 1.13 \times 10^{-5}\ \mathrm{m^2/s}$ is considered as a constant, defining the Schmidt number value as $Sc = \nu_0/D_0 = 1.347$. The Reynolds number value is $Re = v_0 d/\nu_0$, with v_0 being the average inflow velocity.

The honeycomb adsorber consists of multiple parallel narrow channels, and the incoming flow is distributed among these channels. This leads to low values of flow velocities inside the channels, and due to small channel diameters (a few mm or even less) this results in very low Reynolds number values. The flow can therefore be considered as laminar, and it is possible to analytically derive the expression for the velocity profile of the developed flow. The results of such analytical derivation is adopted from derivation of Chen [2], and reads for a channel with a square cross-section as

$$v_x = \frac{48}{\pi^3} v_0 \left(1 - \frac{192}{\pi^5} \sum_{n=1,3,\ldots}^{\infty} \frac{1}{n^5} \cdot \tanh\left(\frac{n\pi}{2}\right)\right)^{-1} \cdot \sum_{n=1,3,\ldots}^{\infty} \frac{1}{n^3} (-1)^{((n-1)/2)} \cdot \left(1 - \frac{\cosh\left(\frac{n\pi y}{d}\right)}{\cosh\left(\frac{n\pi}{2}\right)}\right) \cos\left(\frac{n\pi z}{d}\right) \quad (1)$$

where d is the channel width, v_0 the average inflow velocity and y and z are the coordinates in the channel. It would be possible to compute the flow field by implementing the sub-domain BEM [18], however since preliminary computations showed identical results compared to the results of the analytical expression, the latter was adopted in computing velocity of the fluid inside the channel. This approach substantially decreases the computational time for the simulation and proves reasonable due to the fact that honeycomb adsorption processes are always conducted at low Reynolds numbers.

With a known velocity field, the adsorbate species is transported by the flow by convection and diffusion, according to the following equation:

$$\frac{\partial C}{\partial t} + (\vec{v} \cdot \vec{\nabla}) C = \frac{1}{Re\, Sc} \nabla^2 C, \quad (2)$$

where C is the species concentration, $\vec{v}$ the flow velocity and t the time. Due to very low species concentration in the mixture (less than 1% of the total mass in the flow), the mixture properties are assumed constant, i.e. adsorption and the consequent change of the mixture composition have no effect on the fluid flow.

3.2. Initial and boundary conditions

Geometry of the honeycomb channel in which the adsorption process is taking place is shown in Fig. 1, where a characteristic high ratio between the height and the length of the channel can be observed. The channel height and width in our example are of the same length so the channel cross-section has a square shape. The adsorbent layer on the channel walls is very thin and adsorbate diffusion in the layer is not included in our geometrical and mathematical model.

It is assumed that adsorption equilibrium in the layer is reached instantaneously. The interface between the adsorbent layer and the bulk flow is considered as the boundary of the computational domain, where the no-slip boundary conditions are applied $v_w=0$, with the index w marking the wall of the channel. Adsorbate concentration on the channel wall C_w is set to 0 only in the first time step of the simulation. In the following time steps the value of concentration on the wall C_w is set according to the dynamic model, described in the following section.

At the inflow of the channel the constant concentration $C_{in} = const = 0.007358\ \mathrm{kg/m^3}$ is set and the velocity profile of the developed laminar flow ($Re=2.92$) is applied. At the outflow of the channel the open boundary condition is applied in a manner that concentration values from the nearest nodes inside the domain are copied to the outflow boundary nodes and thus a zero normal flux boundary condition is achieved.

3.3. Concentration boundary condition at the solid wall

The adsorption process in the channel is taking place on the interface between the adsorbent layer and the fluid phase loaded with a low concentration of adsorbate. Molecules of adsorbate are attracted by the adsorbent layer due to the intermolecular forces and when they reach the vicinity of the interface they enter the pore system of adsorbent. By entering the pore system they leave the bulk fluid phase leading to a decrease in the value of adsorbate concentration in the vicinity of the interface. Due to this mechanism a concentration gradient forms from the bulk of the fluid towards the interface

$$\frac{\partial C}{\partial n} < 0 \tag{3}$$

as shown in Fig. 2. Adsorbate concentration gradient causes mass flux of adsorbate molecules towards the adsorbent layer which can be described by the following equation:

$$\dot{q} = \int_{\Gamma} D_0 \vec{\nabla} C \cdot \vec{n}\, d\Gamma \tag{4}$$

Γ is the outer surface area of the adsorbent layer. The quantity of adsorbate mass that can accumulate in the adsorbent layer depends on the adsorption equilibrium at a given concentration and temperature. Adsorption equilibrium can be calculated with the Dubinin–Radushkevich model [3,12]

$$Q_{eq} = q_{max} \exp\left\{ -\left(\frac{RT}{\beta E_0} \ln \frac{C_{sat}}{C} \right)^2 \right\}. \tag{5}$$

In the case of air-butane activated carbon system, the $q_{max} = 509.34\ \mathrm{kg/m^3}$ is the maximum amount of adsorbate adsorbed at the saturation pressure, R is the gas constant, temperature $T = 293.15$ K, $C_{sat} = 6.48\ \mathrm{kg/m^3}$ the saturation concentration, $C = C_{in}$ is the concentration of adsorbate and the affinity coefficient multiplied with the energy parameter is $\beta E_0 = 22\,767$ J/mol.

If the mass flux is calculated with Eq. (4) it is possible to calculate the quantity of accumulated mass in each time step of the simulation with the following equation:

$$Q_{accum}(t) = \sum_{0}^{t} \dot{q} \cdot \Delta t. \tag{6}$$

Mass flux (6) of adsorbate species occurs until the equilibrium state is reached when the accumulated mass of adsorbate Q_{accum} reaches equilibrium mass of adsorbate Q_{eq}. When the equilibrium state is reached the concentration gradient on the wall becomes 0.

The model for defining boundary concentration values (boundary condition) is governing the adsorbate concentration gradient and thus time interval in which equilibrium is reached in the adsorbent layer. The equilibrium state is reached when accumulated mass equals equilibrium mass at given temperature and concentration. Accuracy of channel adsorption process modelling is highly dependable on the model of boundary concentration definition in each time step of simulation. Boundary concentration as a boundary condition can be defined in each time step as

$$C_w = C_i \cdot k(t), \tag{7}$$

where C_i is the concentration value of the nearest numerical mesh node, as shown in Fig. 3, C_w is the boundary concentration on the wall and $k(t)$ is the distribution coefficient in a specific time step.

Other authors [8] used a different approach and set the value of wall concentration $C_w=0$ during the adsorption process. When adsorption equilibrium is reached the wall concentration is set to inlet concentration, $C_w = C_{in}$. A similar approach was also used by Valdes-Solis et al. [23] where an effective diffusion coefficient D_{ef} was proposed for accurate modelling of the adsorption process. We propose to introduce the distribution coefficient $k(t)$ defined as the ratio between accumulated mass and equilibrium mass. It may be written as

$$k(t) = \begin{cases} \dfrac{Q_{accum}}{Q_{eq}} & Q_{accum} \le Q_{eq} \\ 1 & \text{otherwise} \end{cases} \tag{8}$$

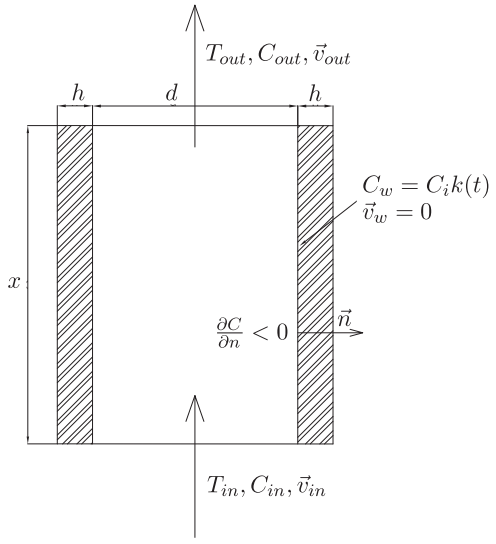

Fig. 2. Definition of concentration boundary conditions.

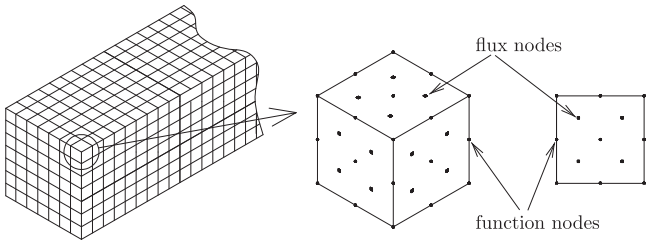

Fig. 3. Surface and volume elements.

4. Numerical method

With the known velocity field the diffusion–convection transport equation for adsorbate species has to be solved numerically. The numerical solution is based on subdomain BEM [17,13] and its extension to 3D problems in the form of the BEM based solution of the velocity–vorticity formulation of the Navier–Stokes equations [18].

Starting with Eq. (2) and applying the Weighted residuals technique the integral form of the adsorbate species conservation equation may be written as

$$c(\vec{\theta})C(\vec{\theta})+\int_\Gamma C\vec{\nabla}u^*\cdot\vec{n}\,d\Gamma=\int_\Gamma u^*\vec{q}_C\cdot\vec{n}\,d\Gamma+Re\,Sc\int_\Omega u^*\{(\vec{v}\cdot\vec{\nabla})C\}d\Omega+Re\,Sc\int_\Omega u^*(\beta_1C+\beta_2C^n+\beta_3C^{n-1})\,d\Omega \tag{9}$$

where $\vec{\theta}$ is the source or collocation point, $\vec{n}$ is a vector normal to the boundary, pointing out of the domain, and u^* is the fundamental solution for the diffusion operator:

$$u^*=\frac{1}{4\pi|\vec{\theta}-\vec{r}|} \tag{10}$$

$c(\vec{\theta})$ is the geometric factor defined as $c(\vec{\theta})=\alpha/4\pi$, where α is the inner angle with an origin in $\vec{\theta}$. If $\vec{\theta}$ lies inside of the domain then $c(\vec{\theta})=1$; $c(\vec{\theta})=1/2$, if $\vec{\theta}$ lies on a smooth boundary. At a time t for a time step Δt a second order finite difference approximation is used to approximate the time derivatives as

$$\frac{\partial C}{\partial t}=\beta_1C+\beta_2C^n+\beta_3C^{n-1} \tag{11}$$

where $\beta_1=3/2\Delta t$, $\beta_2=-2/\Delta t$ and $\beta_3=3/2\Delta t$. C is the concentration in the time step to be computed, C^n and C^{n-1} are the concentrations in the previous two time steps. In the very first time step, when C^{n-1} is not defined, a backward Euler approximation is used ($\beta_1=1/\Delta t$, $\beta_2=-1/\Delta t$ and $\beta_3=0$). Concentrations on the boundary $C(\vec{r})$ and adsorbate mass flux on the boundary $\vec{q}_C(\vec{r})=\vec{\nabla}C(\vec{r})\cdot\vec{n}$ are set as boundary conditions.

It is possible to further simplify the first domain integral in Eq. (9). Due to solenoidality of the velocity field the following relation is valid:

$$(\vec{v}\cdot\vec{\nabla})C=\vec{\nabla}\cdot(\vec{v}C) \tag{12}$$

and the domain term can be transformed into the following form:

$$Re\,Sc\int_\Omega\{(\vec{v}\cdot\vec{\nabla})C\}u^*d\Omega=Re\,Sc\int_\Omega\{\vec{\nabla}\cdot(\vec{v}C)\}u^*d\Omega \tag{13}$$

With the use of the algebraic relation

$$\vec{\nabla}\cdot\{u^*(\vec{v}C)\}=u^*\vec{\nabla}\cdot(\vec{v}C)+(\vec{v}C)\cdot\vec{\nabla}u^* \tag{14}$$

it is possible to further transform the right hand side integral in Eq. (13) into two domain integrals:

$$Re\,Sc\int_\Omega\{\vec{\nabla}\cdot(\vec{v}C)\}u^*d\Omega=Re\,Sc\int_\Omega\vec{\nabla}\cdot\{u^*(\vec{v}C)\}d\Omega-Re\,Sc\int_\Omega(\vec{v}C)\cdot\vec{\nabla}u^*d\Omega. \tag{15}$$

The first integral on the right hand side of Eq. (15) can be transformed into the boundary integral with the use of the Gauss divergence theorem, which finally leads to the transformation of the first domain integral of (9) into the following relation:

$$Re\,Sc\int_\Omega\{(\vec{v}\cdot\vec{\nabla})C\}u^*d\Omega=Re\,Sc\int_\Gamma\vec{n}\cdot\{u^*(\vec{v}C)\}d\Gamma-Re\,Sc\int_\Omega(\vec{v}C)\cdot\vec{\nabla}u^*d\Omega \tag{16}$$

The final form of Eq. (9) can therefore be written with the use of Eq. (16) as

$$c(\vec{\theta})C(\vec{\theta})+\int_\Gamma C\vec{\nabla}u^*\cdot\vec{n}\,d\Gamma=\int_\Gamma u^*\vec{q}_C\vec{n}\,d\Gamma+Re\,Sc\int_\Gamma\vec{n}\left\{u^*(\vec{v}C)\right\}d\Gamma-Re\,Sc\int_\Omega(\vec{v}C)\cdot\vec{\nabla}u^*d\Omega+Re\,Sc\int_\Omega u^*\frac{3C-4C^n+C^{n-1}}{2\Delta t}d\Omega \tag{17}$$

where the second order finite difference approximation of the time derivative was considered.

In order to lower computational demands the subdomain BEM method was used to solve the concentration transport equation. Since Eq. (17) consists of boundary and domain integrals, discretization of only the boundary is not sufficient and discretization of the whole domain is necessary. Computational mesh consists of hexahedral elements which are considered as subdomains, and Eq. (17) is then calculated for each of these subdomains.

The computational domain can be defined as the $\Omega=\sum_e\Omega_e$ and all element sides that are adjacent to the outer domain boundary are denoted as boundary elements, $\Gamma=\sum_b\Gamma_b$. Each subdomain in the form of a hexahedral element consists of 27 nodes. The interpolation is based on continuous quadratic interpolation of the field function with the use of Lagrangian interpolation functions Φ_i. The boundary of each hexahedron subdomain consists of 6 boundary elements and each boundary element consists of 9 function and 4 flux nodes.

With the described discretization Eq. (17) is transformed into the following form for each hexahedron subdomain and for every θ:

$$c(\vec{\theta})C(\vec{\theta})+\sum_b\int_{\Gamma_b}C\vec{\nabla}u^*\cdot\vec{n}\,d\Gamma=\sum_b\int_{\Gamma_b}u^*q\vec{n}\,d\Gamma+Re\,Sc\sum_b\int_{\Gamma_b}\vec{n}\left\{u^*(\vec{v}C)\right\}d\Gamma-Re\,Sc\sum_e\int_{\Omega_e}(\vec{v}C)\cdot\vec{\nabla}u^*d\Omega-Re\,Sc\sum_e\int_{\Omega_e}u^*\frac{3C-4C^n+C^{n-1}}{2\Delta t}d\Omega \tag{18}$$

The concentration function is interpolated over the boundary elements as $C=\sum\varphi_iC_i$ and inside each hexahedron subdomain as $C=\sum\Phi_iC_i$. Flux is interpolated over the boundary elements as $q=\sum\vartheta_iq_i$ using discontinuous linear interpolation scheme, avoiding the definition problems in corners and edges. By applying the described interpolation the following form of the equation (17) can be written:

$$c(\vec{\theta})C(\vec{\theta})+\sum_b\int_{\Gamma_b}\varphi_iC_i\vec{\nabla}\cdot u^*\vec{n}\,d\Gamma=\sum_b\int_{\Gamma_b}u^*\vartheta_iq_i\vec{n}\,d\Gamma+Re\,Sc\sum_b\int_{\Gamma_b}\vec{n}\left\{u^*(\vec{v}\Phi_iC_i)\right\}d\Gamma-Re\,Sc\sum_e\int_{\Omega_e}(\vec{v}\Phi_iC_i)\cdot\vec{\nabla}u^*d\Omega-Re\,Sc\sum_e\int_{\Omega_e}u^*\frac{3\Phi_iC_i-4\Phi_iC_i^n+\Phi_iC_i^{n-1}}{2\Delta t}d\Omega \tag{19}$$

with i denoting the node number.

After the following integrals are calculated:

$$[H]=\int_\Gamma\varphi_i\vec{\nabla}u^*\cdot\vec{n}\,d\Gamma,\quad[G]=\int_\Gamma\vartheta_iu^*d\Gamma,\quad[\vec{A}]=\int_\Gamma\varphi_i\vec{n}\,u^*d\Gamma,\quad[\vec{D}]=\int_\Omega\Phi_i\vec{\nabla}u^*d\Omega\quad[B]=\int_\Omega u^*\Phi_i\,d\Omega. \tag{20}$$

Eq. (19) is transformed into the matrix form:

$$c(\vec{\theta})C(\vec{\theta})+[H]\{C\}=[G]\{q_C\}+Re\,Sc[\vec{A}]\left\{\vec{v}\,C\right\}+Re\,Sc[\vec{D}]\left\{\vec{v}\,C\right\} - Re\,Sc[B]\left(\frac{3\{C\}-4\{C^n\}+\{C^{n-1}\}}{2\Delta t}\right) \quad (21)$$

or in the component form

$$\begin{aligned} c(\vec{\theta})C(\vec{\theta})+[H]\{C\}=&[G]\{q_c\}+Re\,Sc([A_x]\{v_xC\} \\ &+[A_y]\{v_yC\}+[A_z]\{v_zC\}) \\ &-Re\,Sc([D_x]\{v_xC\}+[D_x]\{v_xC\}+[D_x]\{v_xC\}) \\ &-Re\,Sc[B]\left(\frac{3\{C\}-4\{C^n\}+\{C^{n-1}\}}{2\Delta t}\right). \end{aligned} \quad (22)$$

Square brackets in Eq. (22) denote integral matrices and each source point yields one row in these matrices. Because there are 26 function nodes on the boundary of each subdomain (the 27th node is inside the subdomain) there are 26 rows in the matrices $[H]$ and $[\vec{A}]$. Matrices $[\vec{D}]$ have 27 columns since there are 27 nodes for function interpolation in total in every subdomain. Similarly there are 24 columns in the matrix $[G]$ since there are 24 nodes for flux interpolation on the surface of each subdomain.

The Gaussian quadrature algorithm was used for calculating the integrals, which were evaluated in the local coordinate system. A weighted summation of up to 48 integration points on each coordinate axis was used. Free coefficient $c(\vec{\theta})$ is calculated indirectly. Rigid body movement $u=1$, $q=0$ is considered and thus the sum of all $[H]$ matrix elements for each source point is 0. This fact is considered in $c(\vec{\theta})$ calculations and these values are added to the diagonal terms of the $[H]$ matrix. The system is solved in a least squares manner [15].

The accumulated mass in the adsorption process is calculated with Eq. (4) with integration of species fluxes for each boundary element, and a consequent summation in (6). Since the distribution coefficients k are assigned to a boundary element they have to be appropriately distributed to the local nodal values in order to be able to set the correct boundary conditions for the species concentration. The local nodal values of $k(t)$ were computed using a weighted average of all boundary elements that share the chosen node. The weights in the averaging procedure were the area of each boundary element.

4.1. Numerical algorithm

Computation of the adsorption process in the honeycomb channel is based on the derived subdomain based BEM algorithm. Since the channel aspect ratio is very large, the fully developed flow profile was selected for the whole domain and the velocity field was calculated using the analytical expression (1). In the case of mass transfer, the Dirichlet boundary conditions for species concentration at the channel walls, Eq. (7), enabled dynamical adaptation according to the accumulated adsorbate mass on the channel walls. With prescribed concentration boundary conditions and the fully developed flow conditions at the outflow the solution of the species concentration equation (22) gives values of species concentration inside the domain and values of the species fluxes on the channel walls. Once the fluxes are known, computation of accumulated adsorbate mass according to Eq. (6) is done, followed by re-computation of distribution coefficients according to Eq. (8). By obtaining the new boundary concentration values, the computation of the next time step is possible.

The outline of the algorithm can therefore be summarized as

1. initialization, computation of domain and boundary integrals,
2. begin time loop,
3. computation of domain velocity values by solving analytical expression (1),
4. subdomain BEM based solution of the species concentration equation (22), using the known velocity field, for boundary fluxes and domain concentration values,
5. calculation of the adsorption equilibrium for each boundary element with Eq. (5),
6. computation of the mass flux of adsorbate species with Eq. (4),
7. calculation of the distribution coefficient for each boundary element with Eq. (8),
8. transformation of element assigned values of the distribution coefficient to the boundary node based values,
9. calculation of the new boundary conditions for the species concentration on the wall with Eq. (7),
10. end time loop.

5. Results

The adsorption process in a channel of a honeycomb adsorber was experimentally analyzed in [23], where a numerical solution implementing method of lines is also provided. The published results served as a validation test case for determination of the accuracy of our numerical algorithm. In order to have the same model equations the Dubinin–Radushkevich equation for the adsorption equilibrium was selected. The applied equilibrium curve is depicted in Fig. 4.

The computational mesh and time step sensitivity analysis were performed with 6×6 and 8×8 elements in the cross section and 278, 378 and 580 elements in the longitudinal direction. Convergence analysis for the Sherwood number, derived from equating the diffusion mass flux density normal to the wall with the convective mass transfer, defined as

$$Sh=\frac{1}{C-C_{in}}\cdot\frac{\partial C}{\partial n}\cdot d \quad (23)$$

where C is a local concentration, n a normal vector pointing outside of the domain and d is the width of the channel, is depicted in Fig. 5 for the test case of $Re=2.92$ and $Sc=1.34$. Accuracy analysis and computational time considerations led to the decision that the most suitable computational mesh was the $8\times8\times378$ element mesh with 546 215 nodes, as it produces concentration distributions without non-physical oscillations (see, for example, such results for the coarsest mesh in Fig. 5) with relatively low computational demands.

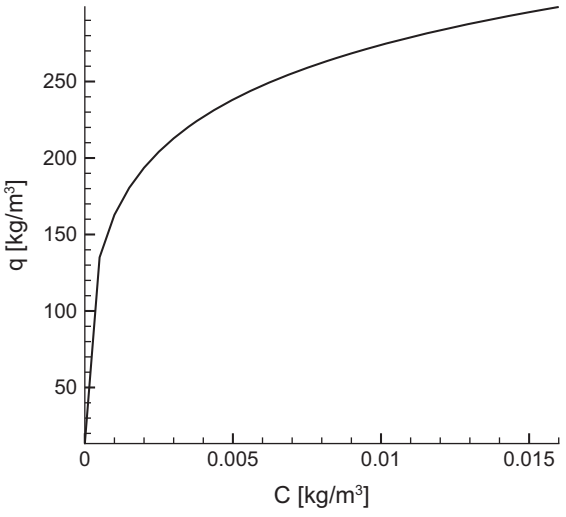

Fig. 4. Equilibrium according to Dubinin–Radushkevich equation.

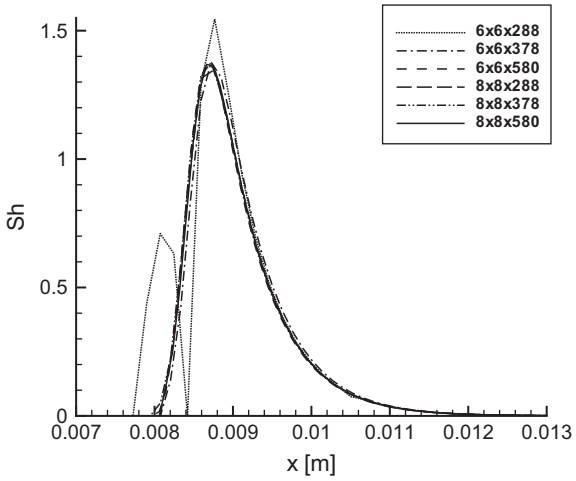

Fig. 5. Computational mesh density analysis with the Sherwood number value distribution along the wall centreline.

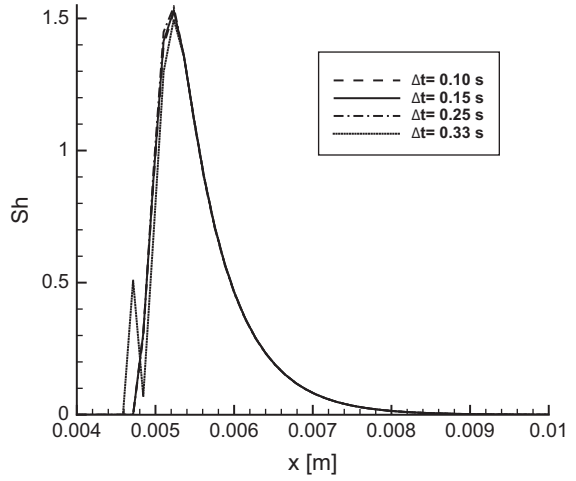

Fig. 6. Sherwood number along the wall centreline, obtained with different time step values.

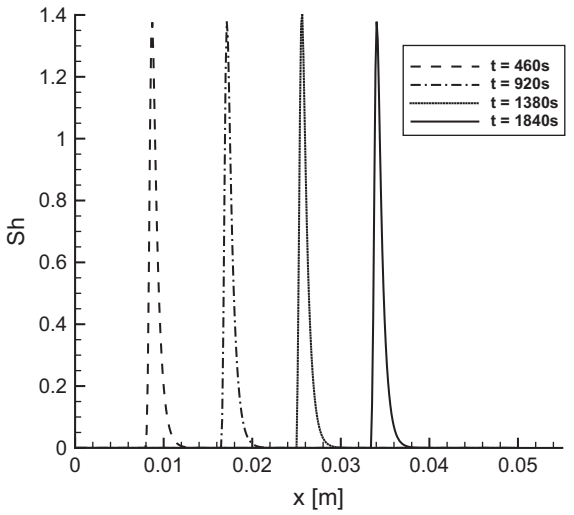

Fig. 7. Temporal development of the local Sherwood number along the channel wall.

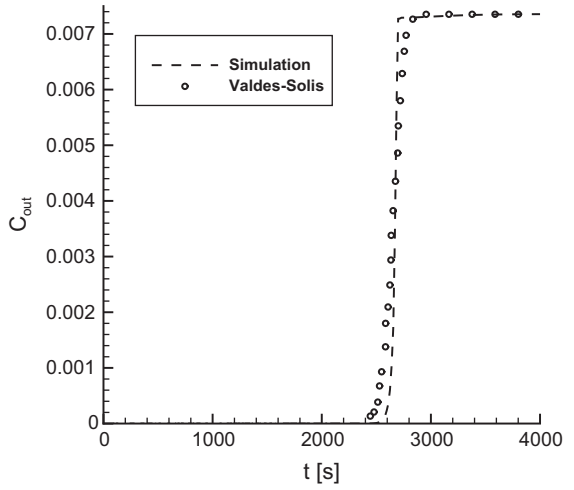

Fig. 8. Comparison of the breakthrough curve between the BEM results and results of Valdes-Solis et al. [23].

According to the selected computational mesh, the time step value analysis was performed, with results shown in Fig. 6 for the case of $Re=2.92$ and $Sc=1.34$ and a preselected position and time instant in the channel. As can be expected, the Sherwood number value increases in front of the concentration front, and then decreases in the bulk of the concentration front, as the accumulated mass on the adsorbent decreases the ability of the adsorbent to adsorb the adsorbate molecules. The smooth transition in the Sherwood number distribution along the x-axis is the result of the appropriate model for the boundary conditions, set by Eq. (7). The largest time step value, that led to accurate computational results, was $\Delta t = 0.25$ s. In terms of the local values of the *CFL* (Courant Friedrichs Lewy) number the value for the $\Delta t = 0.25$ s was $CFL=6.65$. As the concentration front progresses downstream, the adsorption process is affected by this movement. Precisely, the adsorption front, denoted by the highest adsorption fluxes and highest *Sh* number values, moves downstream, as depicted in Fig. 7.

The most important parameter of the adsorption process in a honeycomb adsorber for the engineering use is the breakthrough curve of adsorbate concentration. It is denoted as the time needed for the adsorbate bulk from entering and exiting the channel, and the same can also be concluded for the motion of the adsorption front. This information is crucial for determination of the appropriate time intervals of the adsorption cycle and of the beginning of the regeneration cycle or replacement of the adsorbent. Since the breakthrough curve in a honeycomb adsorber is very steep the information about the breakthrough time is the crucial parameter in the design of the adsorption process. Comparison of the breakthrough curve from the performed BEM simulations with experimental results of [23] for the 200 cpsi–5 cm–5 cm monolith is depicted in Fig. 8. Taking into account that the thermal effects and the diffusion transport inside the adsorbent layer were not considered, a very good agreement is obtained for the nonstationary simulation with computed 15 000 time steps.

In order to analyze the developed numerical algorithm the wall concentration C_w, the distribution coefficient k and the local Sherwood number values were also analyzed. Fig. 7 shows local values of the Sherwood number, proving that the concentration front travels through the honeycomb channel at a constant speed. Concentration front of the adsorbate species develops its shape almost instantly at the beginning of the channel and grows in length almost insignificantly during its passage through the channel length. Fig. 9 shows in detail the local values of the Sherwood number, the wall concentration C_w and the distribution

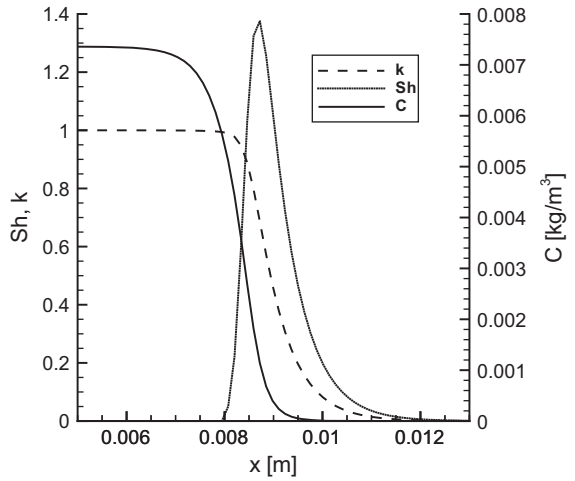

Fig. 9. Local values of partitioning coefficient k, wall concentration C and Sherwood number along the adsorption front.

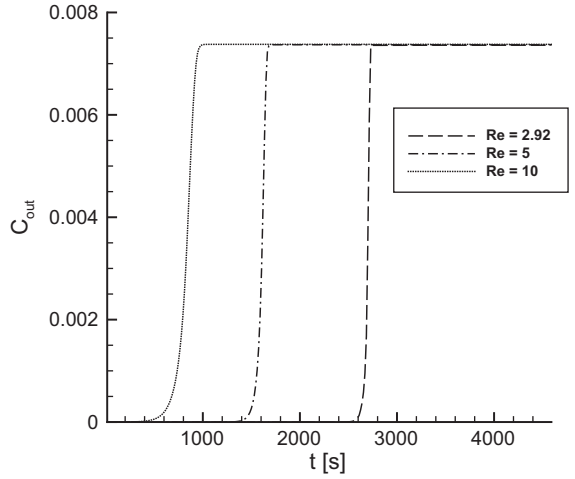

Fig. 10. Breakthrough curves for different values of Reynolds number.

coefficient $k(t)$ in the region of the mass transfer zone (concentration front). The speed of the concentration front propagation in the channel is $v_{front} = 0.00001887$ m/s (case of $Re = 2.92$ and $Sc = 1.34$). Fig. 9 also shows that local values of the Sherwood number decrease much faster in the direction of the inflow than they grow to the maximum value from the outflow direction. Also, the mass transfer and the adsorption processes are occurring in the region with an approximate length of 4 mm or roughly 8% of the entire length of the channel. Local values of wall concentration C_w and distribution coefficient $k(t)$ are very similar with the difference that the concentration curve lags behind the distribution coefficient curve.

When considering industrial applications of honeycomb adsorbers one has to take into account different flow rates that adsorber could be subjected to. Since honeycomb adsorbers are designed for the laminar flow regime the flow rates and hence average velocities in a channel are relatively low. In order to test the adsorption performance under varying flow rate conditions simulations of cases with Reynolds number values 2.92, 5 and 10 were performed. In Fig. 10 the breakthrough curves, representing the average outflow concentration of adsorbate C_{out}, for cases with different Reynolds number values are compared. As could be expected two distinct characteristics can be observed. The breakthrough occurs faster for flows with higher Reynolds number and one can conclude that the time needed for the complete breakthrough of adsorbate ($C_{out} = C_{in}$) is linearly dependable on the flow Reynolds number value. The other main observed characteristic is that due to the higher speed of the flow the concentration front becomes longer and thus the breakthrough curve becomes flatter. This is especially obvious by comparison of the breakthrough curves for the cases of $Re = 10$ and $Re = 2.92$.

The influence of the Reynolds number value on the mass transfer in the region of the concentration front where the adsorption process is occurring can also be clearly observed when comparing the local values of the Sherwood number along the middle of the upper wall of the honeycomb channel, Fig. 11. In order to compare the local values of the Sherwood number the results are shown in one position and are originating from different time instants. It can be seen that the increase in the Reynolds number value causes an increase of the Sherwood number values, hence higher mass transfer rates, accelerating the adsorption process toward the adsorption equilibrium. The other significant effect of the higher Reynolds number value, also observed in Fig. 11, is the increase of the lengths of the mass transfer zone. In the case of $Re = 2.92$ this zone is approximately 4 mm long, and in the case of $Re = 10$ it extends up to 10 mm.

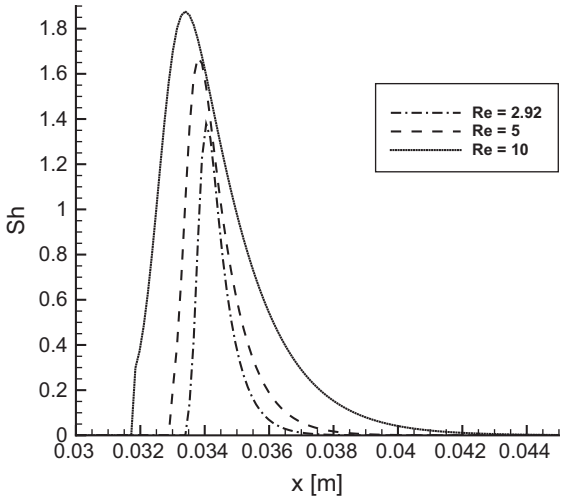

Fig. 11. Comparison of the adsorption front width for different Re number values.

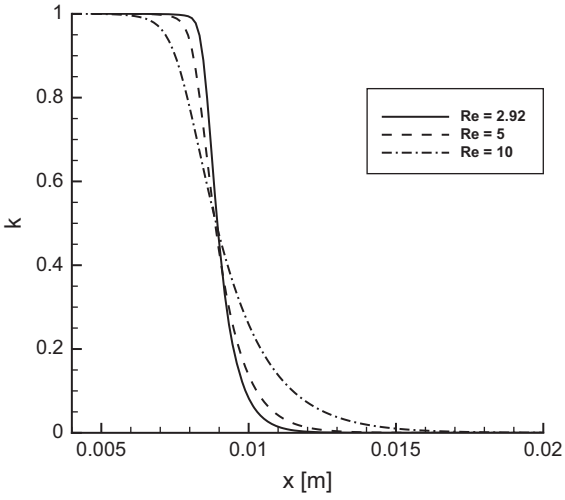

Fig. 12. The k value profiles along the wall centreline for different Re number values.

This fact also explains the flattening of the breakthrough curves with increasing Reynolds number values, Fig. 10.

Finally, the increase in the flow rate and the widening of the active adsorption area has to be accounted for properly by the concentration boundary conditions. As previously discussed, the boundary condition (7) with definition of the distribution coefficient (8) implicitly considers the local concentration conditions, and the distribution of the $k(t)$ values for different time instants, depicted in Fig. 12, proves this fact. With increasing the Reynolds numbers' value the region of mass transfer is longer, effectively widening the area where the distribution coefficient changes its value from 0 to 1.

6. Conclusions

The main aim of the presented work was the development of BEM based mass transfer computational scheme, with the adsorption process dynamics incorporated in the boundary conditions for adsorbate concentration on the adsorbent walls. The presented approach allows a dynamic adaptation of the concentration boundary conditions, effectively leading to a physically more accurate computation of mass fluxes to the adsorbent walls. The latter are computed implicitly by the BEM based solution of the diffusion–convection transport equation for the adsorbate species, which presents a clear advantage over other domain type approximation methods, where the concentration derivatives and hence mass fluxes are computed as a post processing step. The presented numerical scheme was combined with the adsorption equilibrium model in the form of Dubinin–Radushkevich equation, however the equilibrium model can easily be replaced by a more advanced model. The latter option is currently in the process of investigation, with incorporation of the Simplified Local Density equilibrium model [7].

Acknowledgments

The first author acknowledges the partial support of the operation financed by the European Union, European Social Fund, which was greatly appreciated.

References

[1] Alsoy-Akgün Nagehan, Tezer-Sezgin Münewer. DRBEM solution of the thermo-solutal buoyancy induced mixed convection flow problems. Eng Anal Bound Elem 2013;37(3):513–26.
[2] Chen CS. Numerical method for predicting three-dimensional steady compressible flow in long microchannels. J Micromech Microeng 2004;14:1091–100.
[3] Do DD. Adsorption analysis: equilibria and kinetics. London: Imperial College Press; 1998.
[4] Dreisbach F, Staudt R, Keller JU. High pressure adsorption data of methane, nitrogen, carbon dioxide and their binary and ternary mixtures on activated carbon. Adsorption 1999;5(3):215–27.
[5] Dubrowski A. Adsorption—from theory to practice. Adv Colloid Interface Sci 2001;93(13):135–224.
[6] Fedorov A. Combined heat and mass transfer and adsorption dynamics in a honeycomb adsorbent [Ph.D. thesis]. West Lafayette: Perdue University; 1997.
[7] Fedorov A, Viskanta R. Heat/mass transfer and adsorption dynamics in a honeycomb adsorbent: application of the simplified local density model. Thermal Sci Eng 1998;1:1–9.
[8] Fedorov AG, Viskanta R. Analysis of transient heat/mass transfer and adsorption/desorption interactions. Int J Heat Mass Transf 1999;42(5):803–19.
[9] Fitzgerald James E, Robinson Robert L, Gasem Khaled AM. Modeling high-pressure adsorption of gas mixtures on activated carbon and coal using a simplified local-density model. Langmuir 2006;22(23):9610–8.
[10] Gadkaree KP. Carbon honeycomb structures for adsorption applications. Carbon 1998;36(7–8):981–9.
[11] Gadkaree KP, Jaroniec M. Pore structure development in activated carbon honeycombs. Carbon 2000;38(7):983–93.
[12] Gregg SJ, Sing KSW. Adsorption, surface area and porosity. London: Academic Press Inc.; 1982.
[13] Hriberšek M, Škerget L. Boundary domain integral method for high Reynolds viscous fluid flows in complex planar geometries. Comput Methods Appl Mech Eng 2005;194:4196–220.
[14] Kramer J, Ravnik J, Jecl R, Škerget L. Simulation of 3D flow in porous media by boundary element method. Eng Anal Bound Elem 2011;35:1256–64.
[15] Paige CC, Saunders MA. LSQR: an algorithm for sparse linear equations and sparse least squares. ACM Trans Math Softw 1982;8:43–71.
[16] Rangarajan Bharath, Lira Carl T, Subramanian Ramkumar. Simplified local density model for adsorption over large pressure ranges. AIChE J 1995;41(4):838–45.
[17] Ramšak M, Škerget L. A subdomain boundary element method for high-Reynolds laminar flow using stream function—vorticity formulation. Int J Numer Methods Fluids 2004;46:815–47.
[18] Ravnik J, Škerget L, Žunič Z. Combined single domain and subdomain BEM for 3D laminar viscous flow. Eng Anal Bound Elem 2009;33:420–4.
[19] La Rocca A, Hernandez Rosales A, Power H. Radial basis function hermite collocation approach for the solution of time dependent convection–diffusion problems. Eng Anal Bound Elem 2005;29(4):359–70.
[20] Ruthven DM. Principles of adsorption and adsorption processes. New York: Wiley; 1984.
[21] Soule Aaron D, Smith Cassandra A, Yang Xiaoning, Lira Carl T. Adsorption modeling with the ESD equation of state. Langmuir 2001;17(10):2950–7.
[22] Marban G, Valdes-Solis T, Fuertes AB. Preparation of microporous carbon-ceramic cellular monoliths. Microporous Mesoporous Mater 2001;43:113–26.
[23] Valdes-Solis T, Linders MJG, Kapteijn F, Marban G, Fuertes AB. Adsorption and breakthrough performance of the carbon-coated ceramic monolithy at low concentration of n-butane. Chem Eng Sci 2004;59:2791–800.
[24] Wajima Takaaki, Munakata Kenzo, Takeishi Toshiharu, Hara Keisuke, Wada Kouhei, Katekari Kenichi, et al. Adsorption characteristics of water vapor on honeycomb adsorbents. J Nucl Mater 2011;417(1–3):1166–9.
[25] Yates M, Blanco J, Avila P, Martin MP. Honeycomb monoliths of activated carbons for effluent gas purification. Microporous Mesoporous Mater 2000;37(1–2):201–8.
[26] Yates M, Blanco J, Martin-Luengo MA, Martin MP. Vapour adsorption capacity of controlled porosity honeycomb monoliths. Microporous Mesoporous Mater 2003;65(2–3):219–31.
[27] Zhou Chunhe, Hall Freddie, Gasem Khaled AM, Robinson Jr Robert L. Predicting gas adsorption using two-dimensional equations of state. Ind Eng Chem Res 1994;33(5):1280–9.